Smart monitoring of aeronautical composites plates based on electromechanical impedance measurements and artificial neural networks

Pierre Selva, Olivier Cherrier, Valérie Pommier-Budinger, Frederic Lachaud, Joseph Morlier

Smart monitoring of aeronautical composites plates based on electromechanical impedance measurements and artificial neural networks

Pierre Selva [a], Olivier Cherrier [b], Valérie Budinger [c], Frédéric Lachaud [b], Joseph Morlier [b,*]

[a] CT Ingénierie, Toulouse, France
[b] Université de Toulouse, ICA, ISAE, 10 Avenue Edouard Belin, France
[c] Université de Toulouse, Institut Clément Ader, ISAE, UPS, EMAC, INSA, ICA, 10 av. Edouard Belin, F-31055 Toulouse, France

ARTICLE INFO

Keywords:
Composite structures
Structural health monitoring
EM impedance
Neural networks

ABSTRACT

This paper presents a structural health monitoring (SHM) method for in situ damage detection and localization in carbon fiber reinforced plates (CFRPs). The detection is achieved using the electromechanical impedance (EMI) technique employing piezoelectric transducers as high-frequency modal sensors. Numerical simulations based on the finite element method are carried out so as to simulate more than a hundred damage scenarios. Damage metrics are then used to quantify and detect changes between the electromechanical impedance spectrum of a pristine and damaged structure. The localization process relies on artificial neural networks (ANNs) whose inputs are derived from a principal component analysis of the damage metrics. It is shown that the resulting ANN can be used as a tool to predict the in-plane position of a single damage in a laminated composite plate.

1. Introduction

Structural health monitoring (SHM) provide information regarding the condition of a structure in terms of reliability and safety before the damage threatens the integrity of that structure [1,2]. In the paradigm of SHM, there exist five major steps, (a) detection of damage in a structure (b) localization of damage (c) damage identification (d) quantification of damage severity and (e) prognostic of remaining service life of the structure [3]. Aerospace structures are very sensitive to damage since it can lead to major failure. Therefore daily costly inspections are a part of regular maintenance procedures. Nowadays commercial and military aircrafts are increasingly using composite materials to take advantage of their excellent specific strength and stiffness properties but impacts on composites due to bird-strike, hail-storm cause barely visible impact damage (BVID) that underscores the need for robust SHM methods. Hence, damage identification in composites materials is a widely researched area [4–6] that has to deal with problems coming from the anisotropic nature of composites and the fact that much of the damage occurs beneath the top surface of the laminate.

Conventional non-destructive testing (NDT) techniques such as radiographic detection (X-ray) and ultrasound testing (C-Scan) are applicable on composites, but are impractical or very expensive for large components and integrated vehicles. The major advantage of SHM based techniques are their online implementation and their mixed global/local approach (network of sensors).

Vibration based structural health monitoring (VBSHM) technique is also widely used by researchers as an NDT technique. This is a global method to detect, characterize and, to a certain extent, localize damage, based on changes in modal parameters of a structure [7,8]. Variations in the stiffness, mass and damping of a structural system change its frequency–response function and consequently the modal parameters. Recently some authors [9–11] have evaluated experimentally the modal parameters changes due to impacts for several energies of impact. They also demonstrate the sensibility of damping changes to detect delamination in composites structures [9–11]. Frieden et al. proposed a detailed numerical models that take into account damage patterns obtained from X-ray computed topography images. They demonstrate that most of the frequency changes are attributed to a delamination type of damage. An important conclusion is that the total delaminated surface has an affine relation to the absorbed impact energy. A homogenized damage model, including two damage factors allows predicting the change of natural frequencies for a known damage size [12].

Generally vibration-based techniques can be decomposed into two classes [13–16]: data driven approach, and model based approach. Data-driven approaches treat damage identification as a pattern recognition problem. Measured data from the system of

* Corresponding author. Tel.: +33 561338131.
E-mail addresses: pierreselva@gmail.com (P. Selva), olivier.cherrier@isae.Fr (O. Cherrier), valerie.budinger@isae.fr (V. Budinger), frederic.lachaud@isae.fr (F. Lachaud), joseph.morlier@isae.fr (J. Morlier).

interest are assigned a damage class by a pattern recognition algorithm (unsupervised or supervised learning). In supervised learning, examples of all damage classes are required. Model-driven approaches treat damage identification as an inverse problem. First a high-fidelity model of the undamaged structure or system is constructed using physical laws based on first principles. Changes in the measured data are then related to modifications in the physical parameters via system identification algorithms based on linear algebra or optimization theory. Recent advances in SHM tend to couple data-driven techniques with model driven data [17–22]. Especially in composites damage detection area, the current trend is to track changes in damping [10,17] for delamination localization.

For real size industrial structure, the use of smart materials is increasingly gaining popularity among engineering communities [23–28]. In particular, the electromechanical impedance (EMI) based SHM technique possesses distinct advantages, such as the ability to detect incipient damage by using non-intrusive piezoelectric transducers and potentially low-cost applications. The advantage of using piezoelectric sensors for damage detection resides in their high-frequency capability, which exceeds by orders of magnitudes the frequency capability of conventional modal analysis sensors. Thus, these piezoelectric sensors are able to detect changes in the high-frequency structural dynamics at local scale which are directly associated with the presence of incipient damage. Regarding damage detection in composite materials, Gresil et al. [29] applied the EMI method to damage detection in glass fiber reinforced polymer and compared FEM modeling with experimental measurements. In addition, Umesh et al. [30] have shown promising results related to the interaction between the control and diagnostics functions of smart structures equipped with piezoelectricsensors/actuators. Damage indicators derived from the measured electromechanical impedance (EMI) are commonly used to either detect the presence of damage in any structure or provide information about damage localization in a one-dimensional structure [31]. However, as soon as a two-dimensional structure is considered damage indicators based on EMI have difficulties to furnish enough information regarding damage localization. Therefore, in the present paper, artificial neural networks are implemented in order to predict the in-plane damage position in a laminated composite plate. These neural networks are trained using EMI signatures relatives to different localized single damage.

The use of artificial neural networks for damage detection has already been studied by several researchers [32–34]. For example, Giurgiutiu and Kropas-Hughes [32]extracted from EMI resonance frequencies and amplitudes contained in 3 high-frequency spectra (10–40 kHz, 10–150 kHz, and 300–450 kHz). The feature vectors were used as input to a probabilistic neural network. The training was attained using one randomly selected member from each of the 5 damage classes, while the validation was performed on all the remaining members. When the feature vector had a small size, some misclassifications were observed. Upon increasing the size of the feature vector, excellent classification was obtained in all cases. Min et al. [33] proposed the selection of optimal frequency ranges for improving the sensitivity of damage detection, since an improper frequency range can lead to erroneous damage detection results and provide false positive damage alarms. To tackle this issue, they proposed an innovative technique for autonomous selection of damage-sensitive frequency ranges using artificial neural networks (ANNs). Pawar et al. [34] investigated the effect of damage on beams using Fourier analysis of mode shapes in the spatial domains and utilized ANNs trained with Fourier coefficients to detect the damage location and size. All previous works have shown that the implementation of artificial neural networks requires a considerably large set of data to learn a process and also a good choice of inputs to predict the chosen output (in our case the damage localization) with good accuracy. In case of large structures, the amount of required data is quite considerable.

Taking into account these limitations, this article focuses on developing a simple damage model in order to limit the computation time (dependency between high frequency bandwidth and mesh size of FEM model). The domain of damage parameters is explored with few points (100 damage scenario) using Latin Hypercube Sampling for increasing the Neural Networks generalization ability. The originality is to construct local expert (each ANN is constructed for one impact energy) depending on type/class of damage and to study for each class the input parameters dependencies (using classical Principal Components Analysis, PCA). The Probabilistic Neural Networks (PNNs) approach of this article is well adapted to multiscale localization.

Depending on the objectives, focus can be made on global structure (e.g. aircraft door), a subpart (composite plate) or a structural detail like a stiffener.

The proposed methodologyis synthetized in Fig. 1.

Step 1: In order to generate a significant dataset relative to different damage locations, a coupled-field finite-element (FE) model of the structure with the piezoelectric transducers is first developed in commercial software Abaqus [35]. The FE model is created first for a pristine structure and then for a structure with damage. It permits to compute the nodal electrical charges over each transducer electrode, which are then imported into the commercial software Matlab [36] to compute the electromechanical impedance of the structure.
Step 2: The resulting impedance spectrum computed with Matlab is then processed to derive damage indicators. Each damage indicator is computed for each piezoelectric transducer.
Step 3: These damage indicators are used as inputs to train, validate and test the PNN. PNN is used as a classification tool from an a priori zone decomposition of the plate. Several studies with different number and types of inputs have been carried out in order to select the relevant inputs. Final result is a damage location map, which indicates the most probable zone of damage presence.

2. Description on the EMI experimental SET-UP

The structure under study is a composite plate ($200 \times 290\ mm^2$). The composite layup is composed of 12 plies

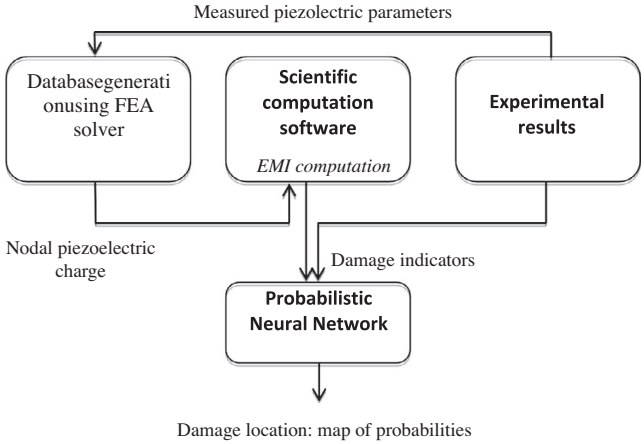

Fig. 1. Flow chart of the proposed method. Finite element models of damage composite plates are used to provide EMI measurements. These EMI signatures are then used to build a database comprised of various damage indicators used as inputs by the probabilistic neural network (PNN). The PNN is then used to predict the damage location in the specimen based on new indicators computed from experimental results.

of carbon/epoxy prepreg T700/M21 with a stratification [45/−45/0/90/0/90]S for a total thickness of 3 mm (Table 1).

Three PI ceramics® type PIC151 of dimensions $10 * 10 * 0.5\ mm^3$ are glued on the plate with an electrical conductive structural glue type EPO-TEK®E4110. The plates are tested clamped on all sides. The location of the piezoelectric transducers is given in Fig. 2.

Five composite plates with piezoelectric ceramics have been manufactured in order to investigate different locations of impact.

Damages are generated by a drop-weight impact tower that permits to measure the velocity and the impact force. Five locations of damage (one per plate) will be investigated. Each plate is impacted between the three transducers with energy of 20 J. It should be noticed that the impact tower forces the impact position to be in the vicinity of the center of the plate (Fig. 3).

The impactor tip has a hemispherical head with a diameter of 12.7 mm. The drop-weight impact tower used in these experiments allows an impact area of $80 \times 40\ mm^2$ so that all the impact points have the same boundary conditions and all the four ends are clamped. A force sensor (type 9051A) provided by Kistler is placed between the impactor tip and the free falling mass of 2 kg. The impact velocity is measured with the help of an optical sensor. The combined weight of the impact head, freefalling mass, force sensor and the accelerometer is 2.03 kg. Further details on the impact test methodology of this drop tower can be found in the reference [6] (see Figs 4 and 5).

In parallel, Ultrasonic control C-scan is carried out for every impact position in order to validate the proposed method. The US-controller is a KRAUTKMARER model USD30 with a frequency scan of 3.5 MHz and a scan resolution of 0.3 mm.

Experimental measurements of the electromechanical impedance are performed before and after the damage for each plate using impedance meter PSM1700.

3. Multiphysics FE model and EMI computation

3.1. Principle of EMI computation from FE model

The finite element model is computed with software Abaqus/Standard and takes into account the composite plate, the piezoelectric transducers, the glue between each sensor and damage.

The composite plate model is comprised of 9300 quadrilateral shell elements with reduced integration and linear interpolation function (S4R element). Low energy impact damage is considered in this article and introduced into the plate model by locally reducing by 80% or 90% both transverse elastic modulus E_2 and E_3 as well as the shear modulus G_{12}, G_{13}, G_{23}.

In Abaqus [35], the piezoelectric behavior is described by equations:

$$\sigma = D^E\varepsilon - e^\Phi E = D^E(\varepsilon - d^\Phi E) \tag{1}$$

$$Q = e^\Phi\varepsilon - D^\Phi E \tag{2}$$

with σ the stress vector (GPa), q the electrical displacement vector (C/m^2), ε the strain vector, E the electrical field vector (V/m), D^E the elasticity matrix (GPa), D^Φ the electric permittivity matrix (F/m) and e^Φ and d^Φ the piezoelectric matrices respectively defined in stress (C/m^2) and strain (m/V) formulation.

The properties of the piezoelectric transducer material (PIC151) given by the supplier are listed in Table 2. The piezoelectric transducers are meshed using 384 C3D2ORE quadratic piezoelectric solid elements.

The glue has a Storage Modulus of 3.75 GPa and is 40 μm thick. The Poisson ratio is chosen equal to 0.35 and the structural damping to 10%. The finite-element model of the glue is comprised of 192 3D-quadratic solid elements.

The method for the electromechanical impedance computation is based on the performing a "direct" steady-state linear dynamic analysis available in software Abaqus/Standard.

In the present case the harmonic analysis is run within the frequency range 10–20 kHz (bandwidth where resonant frequencies can be easily distinguished and measurable), as many times as there are piezoelectric transducers. For each simulation, one transducer is fed with constant voltage V of 1 V in magnitude and the others are maintained to ground. After each simulation, the nodal electric charges at the top electrode of activated piezoelectric patch k are extracted, exported to Matlab and then summed to compute total electrical charge Q_k. Finally intensity in transducer I_k and structure electromechanical impedance Z_k viewed from each activated transducer are derived from the following equations:

$$I_k = i\omega Q_k \tag{3}$$

and

$$Z_k = \frac{V}{I_k} \tag{4}$$

The real part and the imaginary part of the electromechanical impedance can be easily extracted from Eq. (4).

3.2. Model updating

In SHM one of the major issues is the quality of the baseline state in order to compare the dynamic behavior at successive steps (monitoring). In our case, as the baseline is extracted from a FE model, it can be useful to update the model thanks experimental dynamic. Model updating can be defined as adjustment (fit) of an existing FE model which represents the structure under study, using experimental data, so that it more accurately reflects the dynamic behavior of that structure. Model updating can be divided into three steps: (a) comparison and correlation of two sets of data, (b) locating the errors and (c) correcting the errors. Correlation can be defined as the initial step to assess the quality of the FE model. If the difference between the FE model and experimental data is within some preset tolerances, the model can be judged to be accurate and no updating is necessary. A good overview of updating of FE models in structural dynamics has been provided by Friswell and Mottershead [37]. The combination of physical and virtual data plays therefore a relevant role for improved damage diagnostic, mainly if a physical model based approach is performed.

As mentioned in [36] piezoelectric ceramics properties exhibit statistical fluctuations within a given batch and a variance of the order of 5–20% in properties is not uncommon. Therefore model updating is really important to predict the mechanical impedance of the structure with accuracy.

For this purpose, as suggested in [38,39], on one hand the impedance spectrum of every piezoelectric transducer in

Table 1
T700/M21 Properties.

Young Modulus (MPa)			Poisson Ratio			Shear Modulus			Density
E1	E2	E3	μ_{12}	μ_{13}	μ_{23}	G_{12}	G_{13}	G_{23}	ρ
130324	7680	7680	0.33	0.33	0.4	4750	4750	2742	1550

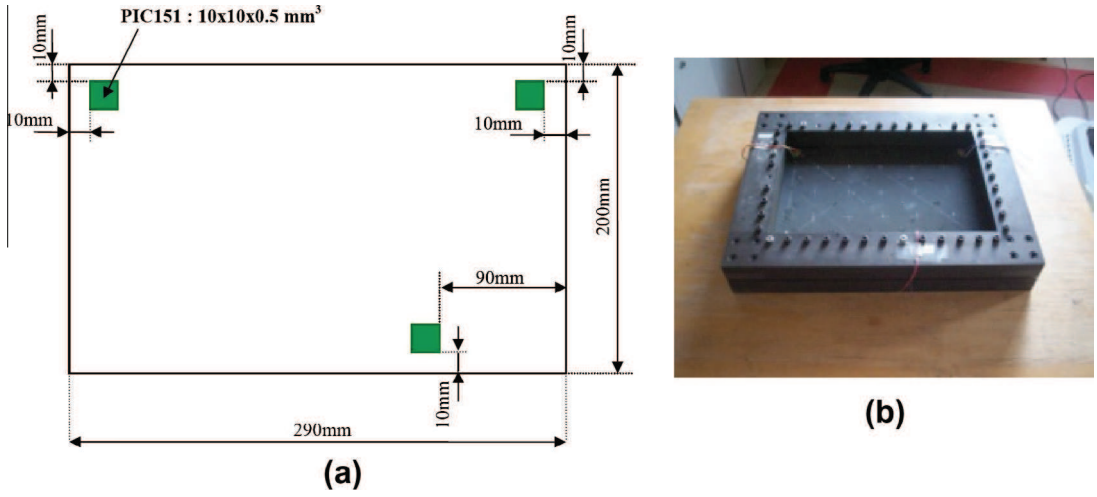

Fig. 2. (a) Schematic representation of the composite structure under study with the unsymmetrical sensors placement (3 PWASs in green squares); and (b) Actual composite plate with clamped edges.

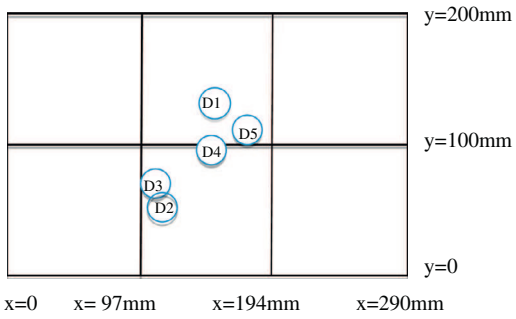

Fig. 3. Distribution of 5 experimental impacts over 5 distinct (but identical) composite plates. 6 clusters (6 squared zones of $100 * 100\,\text{mm}^2$) for the PNN recognition of damage are also highlighted.

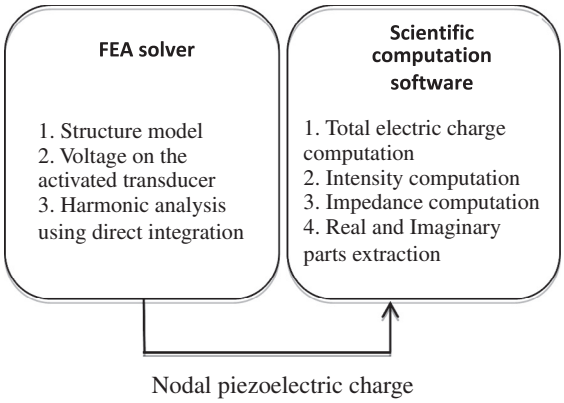

Fig. 4. Principle of EMI computation.

"free-free" condition is recorded and on the other hand, the complex electromechanical admittance for an unbounded piezoelectric wafer active sensor (PWAS) [38,40] is computed:

$$\overline{Y}_{free} = 4\omega j \frac{l^2}{h}\left[\varepsilon_{33}^{T}(1-\delta j) + \frac{2d_{31}^2 Y^E(1+\eta j)}{(1-\nu)}\left(\frac{tanCkl}{kl}-1\right)\right] \quad (5)$$

where l and h are the length and thickness of the patch, Y^E its Young Modulus, ν the Poisson coefficient, ε_{33}^T the dielectric permittivity, δ the dielectric loss factor, η the mechanical loss factor, d_{31} a piezoelectric strain coefficient, k the 2D wave number and C a correction factor.

For low frequencies (typically under 10 kHz), $\frac{tanCkl}{kl}$ tends to 1 and the electromechanical admittance becomes:

$$\overline{Y}_{free-lowfrequencies} = 4\omega\frac{l^2}{h}\varepsilon_{33}^{T}\delta + 4\omega j\frac{l^2}{h}\varepsilon_{33}^{T}. \quad (6)$$

Then, using Eq. (6) and the experimental impedance spectrum, both parameters ε_{33}^T and δ can thus be identified at low frequencies since the spectrum of the imaginary part is proportional to ε_{33}^T and the one of the real part to $\varepsilon_{33}^T\delta$. In Abaqus, the piezoelectric parameter used in the dielectric matrix is ε_{33}^S and not ε_{33}^T. From Eq. (7) derived from matrix relation 8 allows one to compute ε_{33}^S.

$$[\varepsilon^T] - [\varepsilon^S] = [d][e]^T \quad (7)$$

which leads to Eq. (8):

$$\varepsilon_{33}^S = \varepsilon_{33}^T - (2d_{31}e_{31} + d_{33}e_{33}) \quad (8)$$

Concerning parameters d_{31}, η and C, they are identified near the natural frequency of each piezoelectric transducer – which is in the present case close to 170 kHz – using a non-linear curve fitting technique based on the Levenberg–Marquardt algorithm.

This updating method has been performed for every transducer of the experimental set-up. It is illustrated in Fig. 5 for the transducer no.1.

The results of the identification stage are listed for the three transducers in Table 3.

Finally Fig. 6 shows the EM impedance signatures for a pristine structure acquired during an experimental measurement with an impedance analyzer and predicted by the FE model.

Electromechanical resonance peaks are well distinguished. It is also apparent that the simulation results compare very well with the experimental measurements, especially in case of frequency. However, a shift in magnitude can be observed. This can be explained by the inaccuracy in modeling damping and bonding layer [42] and also by the fact that dielectric losses are not taken into account in the FE model as this phenomenon is not yet implemented in the commercially FE package Abaqus.

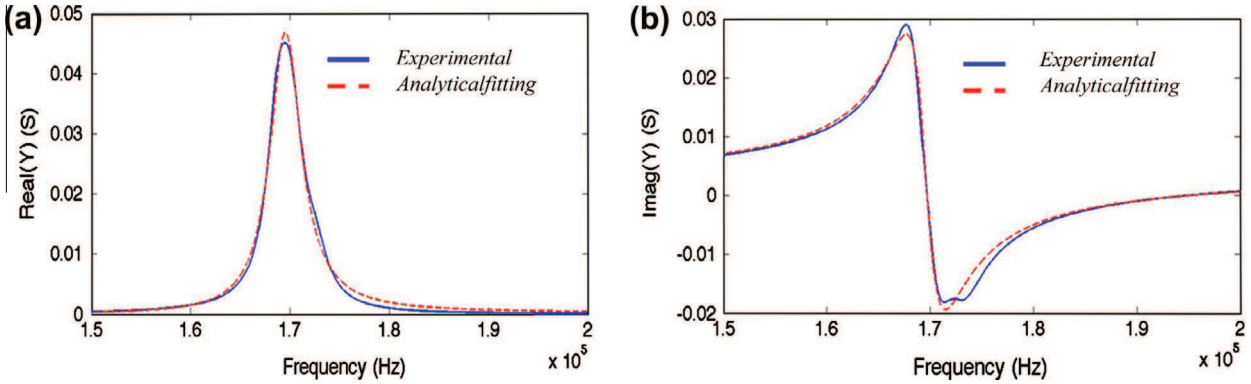

Fig. 5. Experimental and calculated admittance spectra for PWAS no.1 in free-free condition: (a) Real part of admittance vs. frequency. (b) Imaginary part of admittance vs. frequency.

Table 2
PIC151 properties (PI data).

Elasticity matrices

$$[D^E] = \begin{bmatrix} C_{11}^E & C_{12}^E & C_{13}^E & 0 & 0 & 0 \\ C_{12}^E & C_{11}^E & C_{12}^E & 0 & 0 & 0 \\ C_{13}^E & C_{12}^E & C_{33}^E & 0 & 0 & 0 \\ 0 & 0 & 0 & C_{44}^E & 0 & 0 \\ 0 & 0 & 0 & 0 & C_{55}^E & 0 \\ 0 & 0 & 0 & 0 & 0 & C_{66}^E \end{bmatrix} \text{GPa}$$

$$[D^E] = \begin{bmatrix} 107.6 & 63.12 & 63.85 & 0 & 0 & 0 \\ 63.12 & 107.6 & 63.85 & 0 & 0 & 0 \\ 63.85 & 63.85 & 100.4 & 0 & 0 & 0 \\ 0 & 0 & 0 & 22.24 & 0 & 0 \\ 0 & 0 & 0 & 0 & 19.62 & 0 \\ 0 & 0 & 0 & 0 & 0 & 19.62 \end{bmatrix} \text{GPa}$$

Dielectric matrices

$$[D^\Phi] = \begin{bmatrix} \varepsilon_0\varepsilon_{11}^S & 0 & 0 \\ 0 & \varepsilon_0\varepsilon_{11}^S & 0 \\ 0 & 0 & \varepsilon_0\varepsilon_{33}^S \end{bmatrix} = \begin{bmatrix} 9.8235 & 0 & 0 \\ 0 & 9.8235 & 0 \\ 0 & 0 & 7.54 \end{bmatrix} 10^{-6}\ \text{F/m}$$

Piezoelectric matrices

$$[d] = \begin{bmatrix} 0 & 0 & 0 & 0 & d_{15} & 0 \\ 0 & 0 & 0 & d_{15} & 0 & 0 \\ d_{31} & d_{31} & d_{33} & 0 & 0 & 0 \end{bmatrix} = \begin{bmatrix} 0 & 0 & 0 & 0 & 6.1 & 0 \\ 0 & 0 & 0 & 6.1 & 0 & 0 \\ -2.14 & -2.14 & 4.23 & 0 & 0 & 0 \end{bmatrix} 10^{-6}\text{C/N}$$

$$[d] = \begin{bmatrix} 0 & 0 & 0 & 0 & e_{15} & 0 \\ 0 & 0 & 0 & e_{15} & 0 & 0 \\ e_{31} & e_{31} & e_{33} & 0 & 0 & 0 \end{bmatrix} = \begin{bmatrix} 0 & 0 & 0 & 0 & 12 & 0 \\ 0 & 0 & 0 & 12 & 0 & 0 \\ -9.6 & -9.6 & 15.1 & 0 & 0 & 0 \end{bmatrix} \text{C/m}^2$$

Density

$\rho = 7760\ \text{kg/m}^3$

Table 3
Results of the identification of the piezoelectric properties for each sensor.

	PWAS no.1	PWAS no.2	PWAS no.3
$\varepsilon_{33}^T(\times 10^{-8})$	1.991	2.034	2.009
δ	0.0203	0.0207	0.0204
η	0.0224	0.0185	0.0219
$d_{31}(\times 10^{-10})$	−1.837	−1.772	−1.772
C	0.868	−.859	0.881
$\varepsilon_{33}^S(\times 10^{-8})$	0.999	1.055	1.03

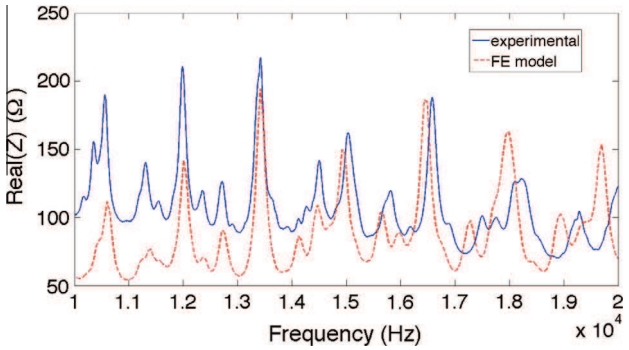

Fig. 6. Comparison of the real part of the impedance frequency response (experimental vs. numerical model) for a pristine composite plate measured from PWAS no.1.

4. Localization of damage using PNN

4.1. Understanding the damage effect through parametric tests

The E/M impedance method is especially effective at ultrasonic frequencies, which properly capture the changes in local dynamics due to incipient structural damage. In a complex aeronautical structures like aircraft door for example, such changes are too small to affect the global dynamics and hence cannot be readily detected by conventional low-frequency vibration methods. Theoretical developments [41] and experimental demonstrations have shown that the real part of the high frequency impedance spectrum is directly affected by the presence of damage or defects in the monitored structure.

Fig. 7 compares the plots of impedance spectra predicted by FE simulations between a pristine and a damage composite plate for two different surfaces of damage – 225 mm^2 and 600 mm^2 – along with two damage severities (elastic properties reduction of 80% or 90%).

This figure clearly demonstrates the ability of the E/M impedance technique to detect the presence of a defect within the structure. Parametric tests help us to understand the EMI variations due to damage. For example complex phenomena such as resonant frequency shifts, peaks splitting as well as appearance of new resonances appeared in our tests.

A way to simply quantify EMI variations is to compute damage indicators extracted from the electromechanical impedance variation between a pristine and damaged structure. Our feature-based method inspired from Giurgiutiu and Kropas-Hughes [32] use a two-stage approach: first, the spectral features (so called damage indictors or damage metrics) that are likely to be affected by damage are extracted. The second step, the features vectors associated with each spectrum are compared using a vector classification technique. We propose a method based on probabilistic neural network (PNN) in order to localize a single damage from features extracted from EMI spectrums. The originality is to train different database in order to be able in a next research works to the damage severity and energy of impact.

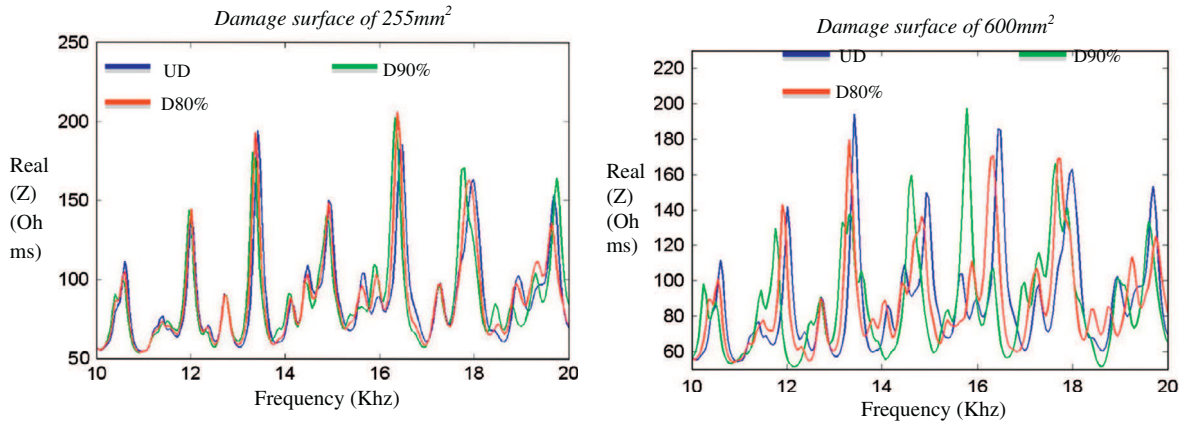

Fig. 7. Comparison of impedance spectra predicted by the FE model at the PWAS no.1 terminals between undamaged (UD) and damaged (D80% or D90%) composite plates. (a) and (b) Plots corresponding to a damage surface of 225 mm^2 and 600 mm^2 respectively.

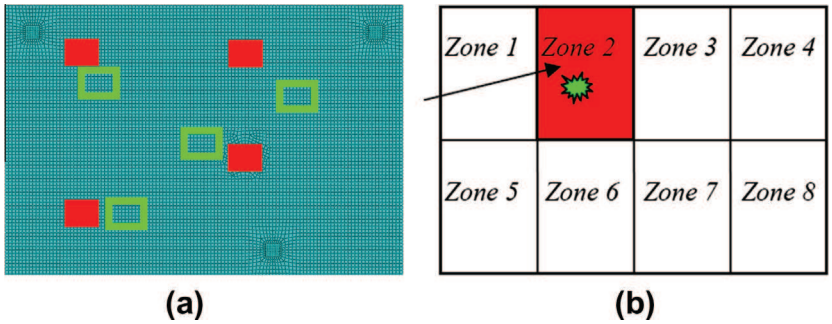

Fig. 8. Comparison of two localization method. (a) ANN produces an estimation (green square) of the real damage localization (red square) from a database of examples. (b) PNN is a problem of classification: the output is the probability that the damage belong to a zone (2 in this example). (For interpretation of the references to color in this figure legend, the reader is referred to the web version of this article.)

4.2. PNN method

PNNs are commonly used for classification problems and they constitute a direct continuation of the work on Bayes classifiers. PNN differs from ANN. In our case, for the prediction of the localization of a single damage, ANN would give a discrete prediction (a couple of coordinates for the damage center) and it has been shown that they may induce large errors for small delamination zones [41]. PNN (from an a priori clustering of the damage location) give a probability map with a zone where the damage belongs (Fig. 8).

PNN have been chosen for the damage localization method because the PNN algorithm is more robust and well adapted to industrial constraints and to our multilevel approach [41]. Moreover, examples close to the cluster border zones are deleted from the database in order to avoid appearance in numerous clusters at the same time.

Basically, a PNN is comprised of two hidden layers: a radial basis layer and a competitive layer. The former computes the distance from the input vector to the training input vectors and produces a vector whose elements indicate how closely the input is matched to a training input. These contributions are then summed for each class of inputs to produce a vector of probabilities. The second layer picks the maximum of these probabilities and returns the associated class.

PNNs possess some useful characteristics such as:

- learning capacity: it captures the relationships between given training examples and their given classification;
- generalization ability: it identifies the commonalities in the training examples and allows to perform classification of unseen examples from the predefined classes.

A simple illustrative example is presented on Fig. 9.

4.3. Damage metrics

A critical point in the generalization process of PNN is the selection of pertinent inputs. First, 7 damage indicators have been selected from bibliography [41] to measure the deviation between the EMI spectra in 2 successive states (damaged/pristine). They are all computed for each of the three piezoelectric ceramic, so 21 indicators are available as inputs of the network.

The 7 damage indicators are defined as:

- Correlation Coefficient of Re(Z).
- Area substraction on both Re(Z) and Im(Z).
- RMS or quadratic mean on both Re(Z) and Im(Z).
- Root Mean Square Deviation on Re(Z) and Im(Z)) defined as:

$$RMSD = \sqrt{\frac{\sum_N [\mathrm{Re}(Zi) - \mathrm{Re}(Z_i^0)]^2}{\sum_N [\mathrm{Re}(Z_i^0)]^2}} \tag{9}$$

For instance, RMSD coefficients provided by each PWAS relative to three surfaces of damage – located at the same position – are depicted in Fig. 10.

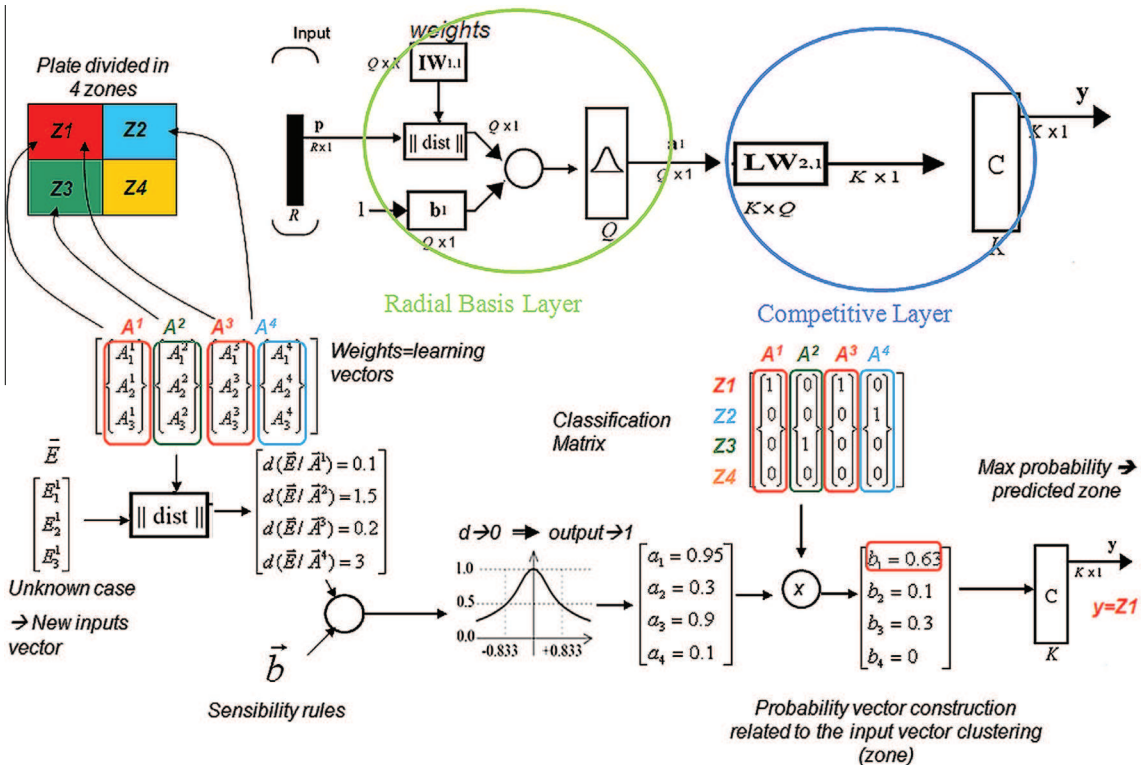

Fig. 9. Simple example of PNN classification from a plate divided in 4 zones (clusters). Four learning vectors A^1–A^4 are used to train the network. The distance between a new input vector E and each learning vector is computed and then passed through a radial basis layer (RBL). A distance close to zero, which means the input vector and the corresponding learning vector are very close, involves an output value from the RBL close to unity. The multiplication of the RBL outputs by a classification matrix provides a probability vector. The transfer function C of the competitive layer retains the highest probability that indicates the localization of the input in the plate.

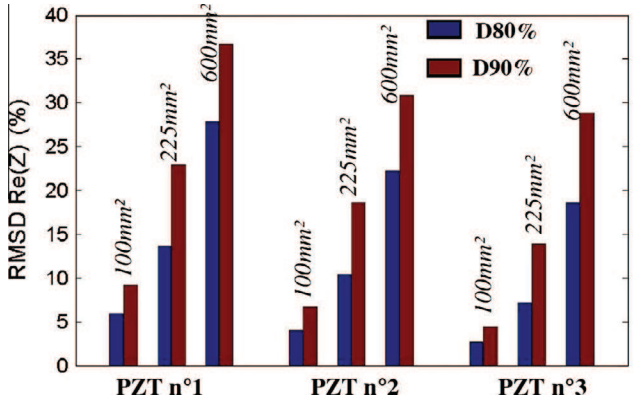

Fig. 10. As it can be expected, the higher the surface of damage, the higher the RMSD index is. The same conclusion can be drawn as regard the damage severity.

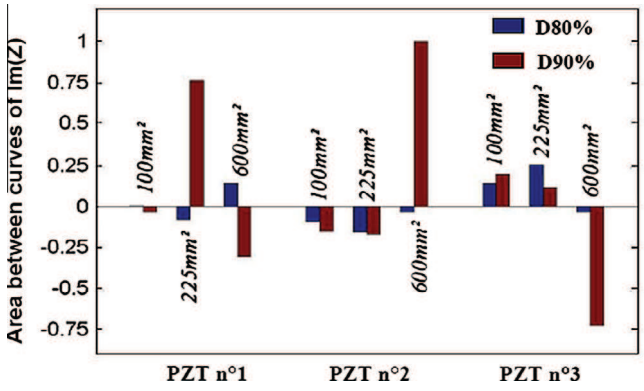

Fig. 11. The other selected indicators more complex behavior that will help PNN to distinguish between damages having similar RMSD value but different localization.

As it can be expected, the higher the surface of damage, the higher the RMSD index is. The same conclusion can be drawn regarding the damage severity. The other selected indicators have more complex behavior that will help PNN to distinguish between damages having similar RMSD value but different locations (Fig. 11).

5. Numerical validation

In the following three damage surfaces of 100 mm^2, 225 mm^2 and 600 mm^2 and two damage severities (elastic properties reduction of 80% or 90%) are considered. Hence three PNNs (each dedicated to one damage surface) are created. For each case, more than 150 positions of damage are generated using a Latin Hypercube Sampling (LHS) method to ensure a random distribution (Fig. 12).

Numerical simulations associated to each damage position are then carried out to generate a database consisting of numerical E/M impedance signatures. Subsequently, each PNN is trained and validated using random input vectors taken from the dataset so as to ensure a good capability of generalization. Finally, the trained neural networks are tested using samples partitioned from the main dataset. The testing data is not used in training and hence provides an "out-of-sample' dataset to test the network. This gives a sense of how well the network is doing. In the present case 90% and 10% of the data are used for the training and testing of the network respectively (see Fig. 13).

It turns out that networks are able to correctly predict the position of fifteen new "numerical" damages (10% of the dataset).

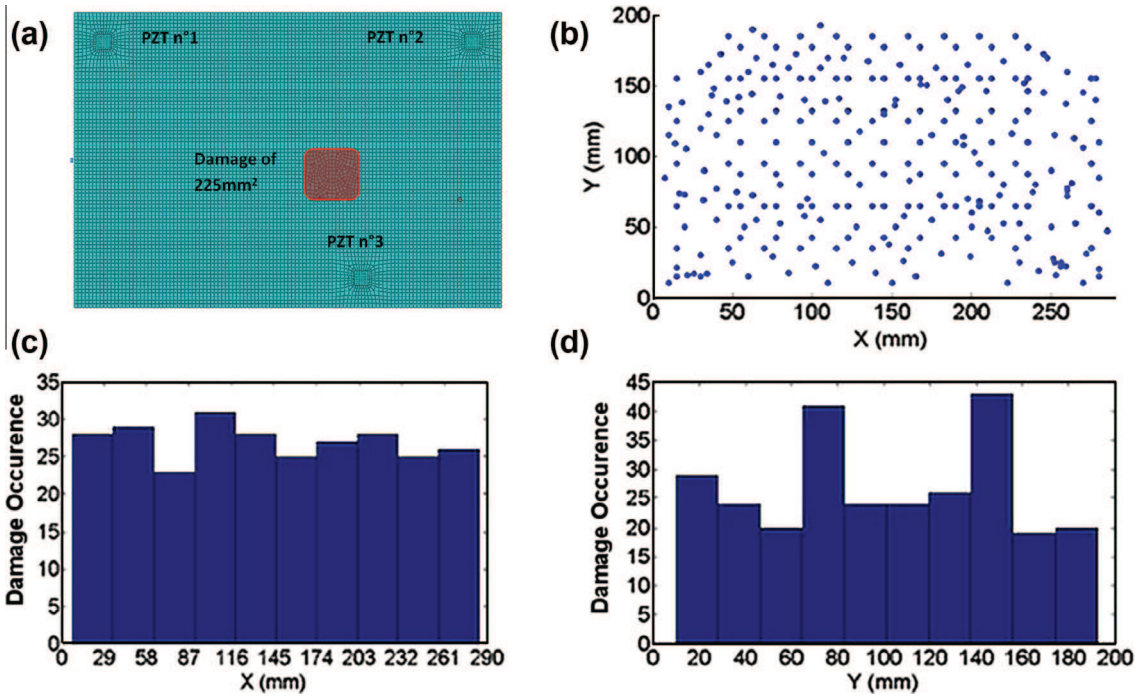

Fig. 12. Example of damages repartition over the composite plate generated from a Latin hypercube sampling method. (a) Visualization of damage positions. (b) and (c) Number of damages in each equally spaced interval along the X and Y axis respectively.

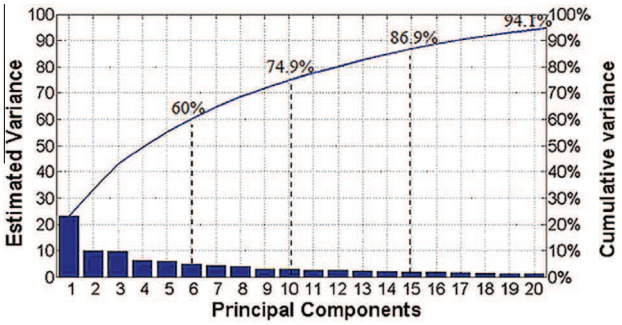

Fig. 13. A statistical approach (PCA) permits to reveal the most sensible variable on the output response. It is shown that 20 principal components can be used to capture 94% of the information (instead of using 43 indicators).

Table 4
Model Based sensitivity, Relationship between damage size and damage estimation (Network performance) using 4 clusters (a quarter of plate). For example we test the highest damage area with only 118 damages in the learning base, we do not use frequency shifts as input vectors and for the test base of 20 unknown (new) cases, we obtain 69% of the networks can predict 90% of the unknown (new) damage location and 90% of the networks can predict 80% of the unknown (new) damage location.

Damage area (mm^2)	Learning/ test examples	Indicators	Network performance at 90%	Network performance at 80%
600	118/20	21	69%	90%
225	245/20	43	61%	85%
100	165/20	43	35%	–

Finally we evaluate the network performance using the 5 best networks over 100.

For high damage area, Table 4 reveals that, the network is able with few exceptions to recognize new damage with good confidence, for example, 90% of the networks can predict 80% of the unknown (new) damage location. So in this case a high variation of the 21 classical indicators can be achieved in which some indicators are correlated.

For medium damage area, preliminary tests have shown that 47% of the networks are able to well classify 90% of new damage with these 21 indicators. To increase the generalization abilities of the network, we add 24 new indicators based on 8 resonant peaks frequency shifts per PWAS:

The frequency shift is defined as:

$$\Delta f_n^D(\%) = |f_n^D - f_n^{UD}|/f_n^{UD} * 100\% \quad (10)$$

where f_n^D is the modal frequency of the damaged structure for the mode n, f_n^{UD} is the modal frequency of the undamaged structure for the mode n.

In order to reduce the size of the input vector while keeping maximum information, a Principal Component Analysis (PCA) is conducted on our dataset. PCA involves a mathematical procedure that transforms a number of possibly correlated variables into a smaller number of uncorrelated variables called principal components. The first principal component accounts for as much of the variability in the data as possible, and each remaining succeeding component accounts for as much of the remaining variability as possible. As it is indicated in Fig. 14, twenty principal components – instead of 45 inputs – can be used to well approximate the outputs (94.1% of the information provided by the 45 inputs is captured).

Due to computational time limits only 200 scenarios were undertaken, but the network performance has much increased: 85% of the networks are able to predict 80% of the 20 new unknown damages.

For small damage area, lower performance of the networks is obtained. Only 35% of the networks are able to localize the damage. The major problem is a damage size dependency in the learning process.

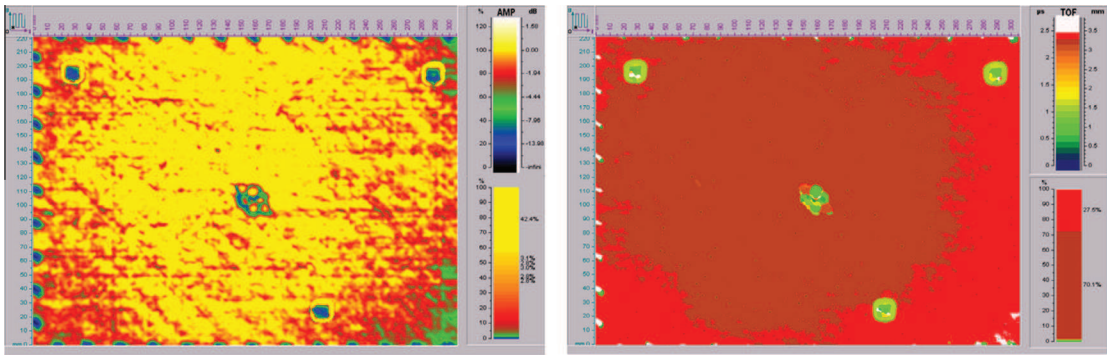

Fig. 14. Ultrasound (Cscan) results for 2 different method (amplitude, deep) reveals the position of PWAS (3 circle) and the position of the D1 damage (center).

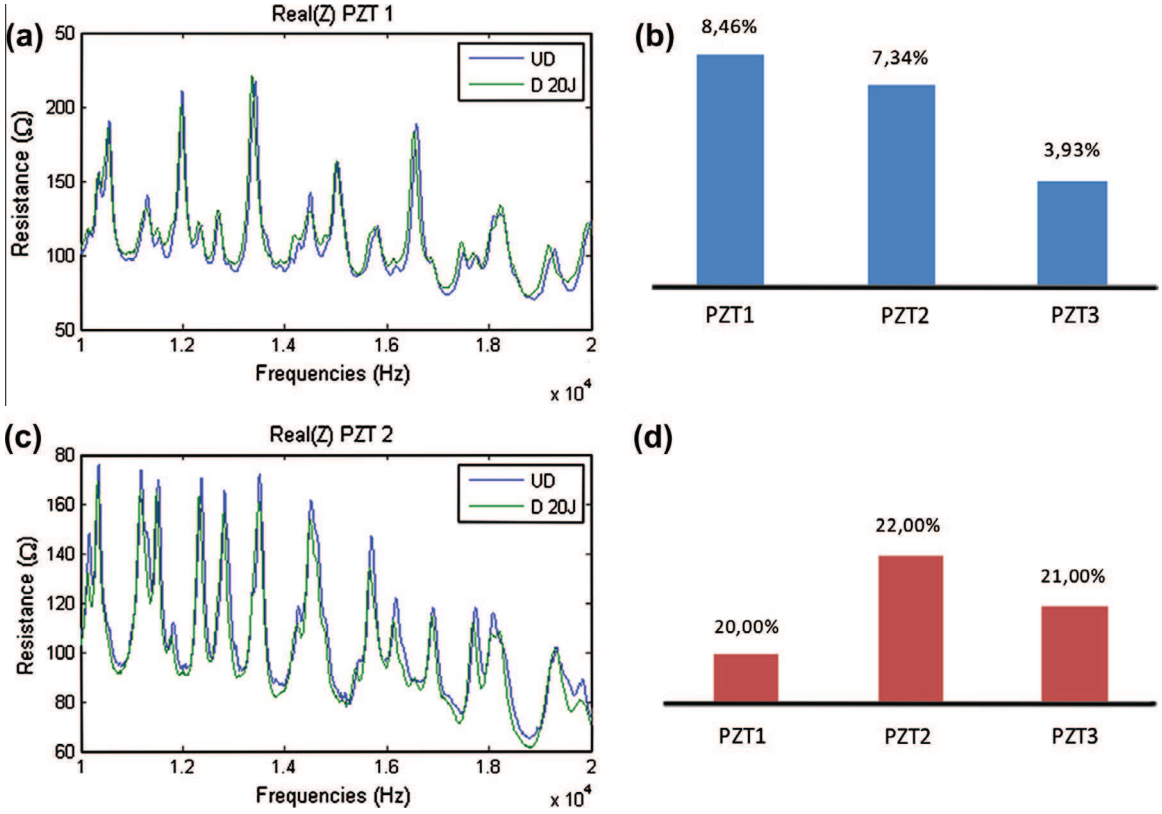

Fig. 15. Comparison of 2 structural state (Damaged, Undamaged), Real(Z) of PWAS 1 (a) and PWAS 2 (c) for D1 case and variation of 2 indices RMSD (b) and frequency shift (d) between the two states: both are Inputs for the PNN approach.

Table 5
Results of localization predictions provided by the PNN trained for 600 mm^2 damage surface.

Plate no.	Damage center (x,y)	US surface (mm^2)	Real zone	Predicted zone
1	(150,145)	≈280	2	2
2	(116,52)	≈381	5	4
3	(110,87)	≈399	5	5
4	(145,95)	≈380	5	5
5	(177,105)	≈366	2	4

It means that all our chosen damage indicators are in this case uncorrelated. Two explanations can conduct to this poor generalization performance: the database is being too small, and more generally very small indicators shifts are obtained.

6. Experimental validation

The primary objective is now to test the PNN approach with experimental data, i.e. experimental damage metrics calculated from experimental E/M impedance spectra. In order to compare to supervised data, we did some Non-Destructive Tests (NDT) illustrated on Fig. 14.

Impedance measurements for each damaged plate are then performed and the corresponding damage metrics are calculated. Fig. 15 shows an example of measurements on the 2 states of the structure (damaged, undamaged) and also 2 indicators shifts for the 3 PWASs for damage case 1.

Finally, these experimental damage indicators are presented to each of the PNN.

Regarding the PNN trained for 225 mm^2 damage surface, predictions in terms of localization were unsatisfactory. This is primarily due to the fact that experimental delamination surfaces are higher than 225 mm^2. This causes experimental damage metrics to be out of bounds of the learned numerical damage indicators. However, the PNN trained for 600 mm^2 surface damages is able to accurately predict the location of 3 out of 5 experimental damages, even for damage surfaces lower than 600 mm^2 (Table 5). Hence, it can be concluded that the closer of the damage surface a PNN is trained for, the better the predictions should be.

7. Conclusion

EMI measurements combined with PNN permit to detect and localize damage in composites carbon fiber reinforced plates. Method presented in this article is original as a coupled FEM approach for updating the baseline model using experimental/numerical EMI correlation is used. This preprocessing limits the potential errors and help us to have confidence in our baseline model, so piezo updating is the most important phase in the monitoring process.

From this realistic baseline model, numerical simulations are then performed so as to generate a significant database relative to various damage scenarios. Using damage indicators calculated from the impedance signature of a pristine and damaged plate, it is shown that the EMI technique performs very well for damage detection. Subsequently, probabilistic neural networks are trained using the numerical database and utilized to estimate the location of a damage previously detected. An important conclusion is also that damages due to small energy of impact needs a high database of examples, in order to obtain a good localization using PNN. Experimental results show that PNNs can be used as a tool to predict the in-plane position of a single damage in a laminated composite plate, as long as real or experimental damage surfaces are lower than numerical damage surfaces the PNN have been trained for. As the damage surface is position dependent, another approach consisting in training PNNs with iso-impact energy – instead of iso-damage surface – should be carried out. However this would require a large set of experimental impact trials to characterize with accuracy the evolution of damages surface over the plate. The damage recognition through PNN is dependent of the initial clustering. Further works will also focus on the development of a hierarchical PNN and in the enhancement of the diagnosis by adding a second output – related to damage severity – to the network. Another perspective resides in the localization of multiple site damages within the structure.

Acknowledgments

The authors would like to acknowledge the Région Midi-Pyrénées, the DIRRECTE as well as the FEDER for the funding of this study through EPICEA 2009 program related to the project titled "SAPES COMPOSITES". We also thank N. Boudjemaa, LATECOERE, for his insightful comments.

References

[1] Farrar CR, Worden K. An introduction to structural health monitoring. Philos Trans R Soc A 2007;365:303–15.
[2] Doebling SW, Farrar CR, Prime MB. A summary review of vibration-based damage identification methods: identification methods. Shock Vib Digest 1998;30:91–105.
[3] Farrar CR, Lieven AJ. Damage prognosis: the future of structural health monitoring. Philos Trans R Soc A 2007;365:623–32.
[4] Schubel PM, Luo JJ, Daniel IM. Impact and post impact behaviour of composite sandwich panels. Composites Part A 2007;38:1051–7.
[5] Abrate S. Impact on composite structures. Cambridge University Press; 1988.
[6] Petit S, Bouvet C, Bergerot A, Barrau JJ. Impact and compression after impact experimental study of a composite laminate with a cork thermal shield. Compos Sci Technol 2007;67:3286–99.
[7] Cawley P, Adams RD. The location of defects in structures from measurements of natural frequencies. J Strain Anal Eng Des 1979;14(2):49–57.
[8] Farrar CR, Doebling SW, Nix DA. Vibration-based structural damage identification. Philos Trans: Math Phys Eng Sci 2001;359(1778):131–49.
[9] Montalvão D, Maia NMM, Ribeiro AMR. A review of vibration-based structural health monitoring with special emphasis on composite materials. Shock Vib Digest 2006;38(4).
[10] Shahdin A, Morlier J, Gourinat Y. Correlating low energy impact damage with changes in modal parameters: a preliminary study on composite beams. Struct Health Monit 2009;8(6):523–36. ISSN 1475–9217.
[11] Shahdin A, Morlier J, Gourinat Y. Damage monitoring in sandwich beams by modal parameter shifts: a comparative study of burst random and sine dwell vibration testing. J Sound Vib 2010;3(5):566–84. ISSN 0022-460X.
[12] Frieden J, Cugnoni J, Botsis J, Gmür T. Vibration-based characterization of impact induced delamination in composite plates using embedded FBG sensors and numerical modelling. Compos B Eng 2011;42(4):607–13.
[13] Adams DE. Health monitoring of structural materials and components. Wiley; 2007.
[14] Staszewski W, Boller C, Tomlinson GR. Health Monitoring of Aerospace Structures. Wiley; 2003.
[15] Balageas D, Fritzen CP, Güemes A. Structural health monitoring. ISTE; 2006.
[16] Yan YJ, Cheng L, Wu ZY, Yam LH. Development in vibration-based structural damage detection technique. Mech Systems Signal Proc 2007;21:2198–211.
[17] Montalvao D, Ribeiro AM, Duarte-Silva J. A method for the localization of damage in a CFRP plate using damping. Mech Syst Signal Proc 2008. http://dx.doi.org/10.1016/j.ymssp.2008.08.011.
[18] Moaveni B, He X, Conte JP. Damage identification of a composite beam using finite element model updating. Comput-Aided Civil Infrastruct Eng 2008;23(5):339–59.
[19] Meo M, Zumpano G. Damage assessment on plate-like structures using a global-local optimization approach. Optim Eng 2008;9:161–77.
[20] Niemann H, Morlier J, Shahdin A, Gourinat Y. Damage localization using experimental modal parameters and topology optimization. Mech Systems Signal Proc 2010;24:636–52.
[21] Shahdin A, Morlier J, Niemann H, Gourinat Y. Correlating low energy impact damage with changes in modal parameters: diagnosis tools and FE validation. Struct Health Monit 2011;10(2):199–217.
[22] Viana JC, Antunes PJ, Guimara RJ, Ferreira NJ, Baptista MA, Dias GR, et al. Combining experimental and computed data for effective SHM of critical structural components. In: Aerospace Conference, 2011 IEEE, vol. no. 5–12 March 2011. p. 1–10.
[23] Park G, Sohn H, Farra CR, Inman DJ. Overview of piezoelectric Impedance-based health monitoring and path forward. Shock Vib Digest 2003;35(5):451–63.
[24] Lim Y, Bhalla S, Soh CK. Structural identification and damage diagnosis using self-sensing piezo-impedance transducers. Smart Mater Struct 2006;15(4):987–95.
[25] Wei Yan, Cai JB, Chen WQ. Monitoring interfacial defects in a composite beam using impedance signatures. J Sound Vib 2009;326(1-2):340–52. 25.
[26] Bhalla S, Soh CK. Structural health monitoring by piezo-impedance transducers applications. J Aerospace Eng ASCE 2004;17(4):166–75.
[27] Yan W, Chen WQ. Structural health monitoring using high-frequency electromechanical signatures. Adv Civil Eng 2010:1–11.
[28] Bhalla S, Gupta A, Bansal S. Ultra low-cost adaptations of electro-mechanical impedance technique for structural health monitoring. J Intell Mater Syst Struct 2009;20(8):991–9.
[29] Gresil M, Yu L, Giurgiutiu V, Sutton M. Predictive modeling of electromechanical impedance spectroscopy for composite materials. Struct Health Monit Int J 2012;11.
[30] Umesh K, Ganguli R. Shape and vibration control of a smart composite plate with matrix cracks. Smart Mater Struct 2009;18:2.
[31] Giurgiutiu V, Zagrai A. Damage detection in thin plates and aerospace structures with the electro-mechanical impedance method. Struct Health Monit – Int J 2005;4(9):1025–36.
[32] Giurgiutiu V, Kropas-Hughes C. Comparative study of neural-network damage detection from a statistical set of electro-mechanical impedance spectra, In: SPIE's 10th annual international symposium on smart structures and materials and 8th annual international symposium on NDE for health monitoring and diagnostics. San Diego; 2–6 March 2002.
[33] Min J, Park S, Yun CB. Impedance-based structural health monitoring using neural networks for autonomous frequency range selection. Smart Mater Struct 2010;19:12.
[34] Pawar PM, Reddy KV, Ganguli R. Damage detection in beams using spatial Fourier analysis and neural networks. J Intell Mater Syst Struct 2007;18(4):347–59.
[35] Abaqus user's manual, Dassault System Simulia Corp., Providence, RI; USA, 2008.
[36] Matlab r2010a user's guide, the Mathworks inc., MA, USA; 2010.
[37] Friswell MI, Mottershead JE. Finite element model updating in structural dynamics. Springer; 1995.
[38] Bhalla S, Soh CK. Structural health monitoring by piezo-impedance transducers: modelling. J Aerospace Eng ASCE 2004;17:154–65.

[39] Bhalla S, Soh CK. Structural health monitoring by piezo-impedance transducers: applications. J Aerospace Eng ASCE 2004;17:166–75.
[40] Bhalla S, Soh CK. Electro-mechanical impedance technique for structural health monitoring and non-destructive evaluation. In: National workshop on structural health monitoring, non-destructive evaluation and retrofitting of structures. Indian Institute of Technology Delhi; 2008.
[41] Giurgiutiu V. Structural health monitoring with piezoelectric wafer active sensors. USA: Academic Press – Elsevier; 2008.
[42] Yang Y, Lim YY, Soh CK. Practical issues related to the application of the electromechanical impedance technique in the structural health monitoring of civil structures: II. Numerical verification. Smart Mater Struct 2008;17.